

Dynamical properties of nuclear and stellar matter and the symmetry energy

Helena Pais, Alexandre Santos, Lucília Brito and Constança Providência
*Centro de Física Computacional, Department of Physics
University of Coimbra, 3004-516 Coimbra, Portugal*

The effects of density dependence of the symmetry energy on the collective modes and dynamical instabilities of cold and warm nuclear and stellar matter are studied in the framework of relativistic mean-field hadron models. The existence of the collective isovector and possibly an isoscalar collective mode above saturation density is discussed. It is shown that soft equations of state do not allow for a high density isoscalar collective mode, however, if the symmetry energy is hard enough an isovector mode will not disappear at high densities. The crust-core transition density and pressure are obtained as a function of temperature for β -equilibrium matter with and without neutrino trapping. An estimation of the size of the clusters formed in the non-homogeneous phase as well as the corresponding growth rates and distillation effect is made. It is shown that cluster sizes increase with temperature, that the distillation effect close to the inner edge of the crust-core transition is very sensitive to the symmetry energy, and that, within a dynamical instability calculation, the pasta phase exists in warm compact stars up to 10 - 12 MeV.

PACS numbers: 21.60.-n,21.60.Ev,26.60.Gj,24.10.Jv

I. INTRODUCTION

Understanding the properties of isospin rich nuclear matter is one of the present goals of both nuclear physics and astrophysics. A major scientific effort is being carried out at an international level to study experimentally the properties of asymmetric nuclear systems and probe the behavior of the symmetry energy close to and above saturation density [1]. Astrophysical observations of compact objects are also a window into both the bulk and the microscopic properties of nuclear matter at extreme isospin asymmetries [2]. Measurements coming from both laboratory and astrophysical observations are expected to put constraints on the acceptable properties of the equation of state (EOS) of asymmetric nuclear matter [3, 4].

In the last years an important effort has been done to determine the density dependence of the symmetry energy of asymmetric nuclear matter (see the reviews [1, 2, 4] and references there in). Correlations between different quantities in bulk matter and finite nuclei have been established. Examples are the correlation between the slope of the pressure of neutron matter at $\rho = 0.1 \text{ fm}^{-3}$ and the neutron skin thickness of ^{208}Pb [5], or the correlation between the crust-core transition density and the neutron skin thickness of ^{208}Pb [6]. Both Skyrme forces and relativistic mean-field (RMF) models have been used to describe these correlations. Recently, it was shown that the parameters characterizing

of the different models and a thermodynamic approach to determine the transition density. Many other works have studied the instability of asymmetric matter using a thermodynamical approach [10].

Instead of using a thermodynamic approach, in [11] the transition density was estimated in a local equilibrium approximation by determining the density for which matter becomes unstable to small density fluctuations. It has been shown in [12–15] that the thermodynamical method gives a good estimation of the transition density for cold β -equilibrium matter, although a bit too large. In [13, 14] a comparison was done between the transition density obtained from the Vlasov formalism, a semi-classical limit of the description of the collisionless regime, and a Thomas-Fermi calculation of the pasta phase. It was shown that both results almost coincide: the Vlasov formalism predicts a transition density only slightly smaller than the Thomas-Fermi one. Moreover, Ducoin *et al.* [16] have shown that the transition density obtained within the Vlasov formalism does not differ from the one obtained by [11] using a local equilibrium approximation.

The main goal of this work is to study, in the framework of relativistic models, the effect of the symmetry energy density dependence on some dynamical properties of asymmetric nuclear matter, namely the dynamical instabilities at sub-saturation densities at zero and finite temperature and the isoscalar and isovector collective modes

As shown in [19, 20] the pressure at the inner boundary of the crust defines the mass and moment of inertia of the crust. This establishes a relation between the EOS and compact stars observables. Until now the transition pressure and density have only been studied at zero temperature but it is also of interest to determine how do these quantities depend on the temperature. This will be one of the aims of the present work. The transition density and pressure will be determined from the crossing of the β -equilibrium EOS of stellar matter and the dynamical spinodal. Warm stellar matter may contain trapped neutrinos [21]. We will consider the conditions expected in the inner crust and in the core of a neutron star, namely of isospin asymmetry, density and temperature. This same problem was investigated very recently within a momentum-dependent effective interaction for nucleons [22].

Collective modes in asymmetric nuclear matter have already been studied in previous works [23–28] both within non-relativistic and relativistic nuclear models. These modes corresponding to isospin or density waves in infinitely extended nuclear matter can be identified as the counterpart of giant resonances in the atomic nucleus [23]. They may be of particular importance for the formation of shock waves in nuclear matter [23, 29] and they will affect the thermal properties of neutron stars, since the neutrino mean free paths are affected by the propagation of collective modes in the medium [30].

The authors of Ref.[26] have predicted the existence of a neutron wave at reasonably large densities, for $\rho \sim 3\rho_0$, where ρ_0 is the saturation density. They have also shown that the inclusion of the scalar isovector virtual $\delta(a_0(980))$ field may strongly reduce the restoring force for the isovector collective modes of the system. In a similar way they predict that, if the incompressibility is decreasing with the increase of the density, the exotic high density isoscalar collective modes could disappear. This could be a signature of the softening of the equation of state (EOS) at large densities [26].

In the present work we will study the collective modes of nuclear matter within the Vlasov equation for relativistic nuclear models developed in [31, 32] for symmetric nuclear matter and applied later to asymmetric nuclear matter [27, 28, 33]. It is a semi-classical approach which can be used to determine the eigenmodes of nuclear asymmetric matter and corresponds to the $\hbar \rightarrow 0$ limit of the time dependent Hartree-Fock. The relativistic Vlasov equation for the non-linear Walecka model

that differ in the density dependence of the symmetry energy and the incompressibility. The following models will be considered: NL3 [36] with a quite large symmetry energy and incompressibility at saturation and which was fitted in order to reproduce the ground state properties of both stable and unstable nuclei, TM1 [37] which also reproduces the ground state properties of both stable and unstable nuclei and provides an equation of state of nuclear matter similar to the one obtained in the RBHF (Relativistic Brueckner Hartree-Fock) theory, softer than NL3 at high densities, FSU [38] which was accurately calibrated to simultaneously describe the GMR in ^{90}Zr and ^{208}Pb , and the IVGDR in ^{208}Pb and still reproduce ground-state observables of stable and unstable nuclei. In TM1 a quartic self-interaction ω -meson term was included, which softens the EOS. This term is also present in the FSU parametrization together with a mixed isoscalar-isovector coupling which modifies the density dependence of the symmetry energy. Finally, we also consider NL3 $\omega\rho$ and TM1 $\omega\rho$, the NL3 and TM1 parametrizations with a mixed isoscalar-isovector coupling which we will vary in order to change the density dependence of the symmetry energy [6]. The EOS obtained within NL3 is too hard and well above the limits that collective flow data [39] impose to the EOS of symmetric matter. Also, the symmetry energy slope of NL3 at saturation is 118 MeV slightly above the limit obtained with experimental constraints from isospin diffusion $63 < L < 113$ MeV, and well above other constraints [40]. Nevertheless, we have chosen this model because it has been calibrated to describe the ground-state of a wide number of stable and unstable nuclei and because it is still frequently used. This model is taken as an example of a model with an hard EOS both in the isoscalar and isovector channel.

We will consider both asymmetric nuclear matter, neutral neutron-proton-electron (*npe*) neutrino-free matter in β -equilibrium at zero temperature and *npe* matter with trapped neutrinos in β -equilibrium for a lepton fraction $Y_l = 0.4$, both at zero and finite temperature.

In Sec. II we review the formalism used, in Sec. III we present and discuss the results obtained and finally, in Sec. IV we draw some conclusions.

II. THE VLASOV EQUATION FORMALISM

We use the relativistic non-linear Walecka model

the electromagnetic field A^μ . The Lagrangian density reads:

$$\mathcal{L} = \sum_{i=p,n} \mathcal{L}_i + \mathcal{L}_e + \mathcal{L}_\sigma + \mathcal{L}_\omega + \mathcal{L}_\rho + \mathcal{L}_A$$

where the nucleon Lagrangian reads

$$\mathcal{L}_i = \bar{\psi}_i [\gamma_\mu iD^\mu - M^*] \psi_i,$$

with

$$iD^\mu = i\partial^\mu - g_v V^\mu - \frac{g_\rho}{2} \boldsymbol{\tau} \cdot \mathbf{b}^\mu - eA^\mu \frac{1 + \tau_3}{2},$$

$$M^* = M - g_s \phi,$$

and the electron Lagrangian is given by

$$\mathcal{L}_e = \bar{\psi}_e [\gamma_\mu (i\partial^\mu + eA^\mu) - m_e] \psi_e.$$

The isoscalar part is associated with the scalar sigma (σ) field ϕ , and the vector omega (ω) field V_μ , whereas the isospin dependence comes from the isovector-vector rho (ρ) field b_μ^i (where μ stands for the four dimensional space-time indices and i the three-dimensional isospin direction index). The associated Lagrangians are:

$$\begin{aligned} \mathcal{L}_\sigma &= +\frac{1}{2} \left(\partial_\mu \phi \partial^\mu \phi - m_s^2 \phi^2 - \frac{1}{3} \kappa \phi^3 - \frac{1}{12} \lambda \phi^4 \right), \\ \mathcal{L}_\omega &= -\frac{1}{4} \Omega_{\mu\nu} \Omega^{\mu\nu} + \frac{1}{2} m_v^2 V_\mu V^\mu + \frac{1}{4!} \xi g_v^4 (V_\mu V^\mu)^2, \\ \mathcal{L}_\rho &= -\frac{1}{4} \mathbf{B}_{\mu\nu} \cdot \mathbf{B}^{\mu\nu} + \frac{1}{2} m_\rho^2 \mathbf{b}_\mu \cdot \mathbf{b}^\mu, \\ \mathcal{L}_A &= -\frac{1}{4} F_{\mu\nu} F^{\mu\nu}, \end{aligned} \quad (1)$$

where $\Omega_{\mu\nu} = \partial_\mu V_\nu - \partial_\nu V_\mu$, $\mathbf{B}_{\mu\nu} = \partial_\mu \mathbf{b}_\nu - \partial_\nu \mathbf{b}_\mu - g_\rho (\mathbf{b}_\mu \times \mathbf{b}_\nu)$ and $F_{\mu\nu} = \partial_\mu A_\nu - \partial_\nu A_\mu$.

The model comprises the following parameters: three coupling constants g_s , g_v and g_ρ of the mesons to the nucleons, the bare nucleon mass M , the electron mass m_e , the masses of the mesons, the electromagnetic coupling constant $e = \sqrt{4\pi/137}$ and the self-interacting coupling constants κ , λ and ξ . In this Lagrangian density, $\boldsymbol{\tau}$ is the isospin operator.

The NL3 $\omega\rho$, TM1 $\omega\rho$ and FSU parametrizations also include a nonlinear $\omega\rho$ coupling term, which allows to change the density dependence of the symmetry energy. This term is given by:

Table I shows nuclear matter properties at the saturation density for these models: the binding energy per nucleon E/A , the incompressibility coefficient K , the symmetry energy \mathcal{E}_{sym} , the symmetry energy slope L , the symmetry energy curvature K_{sym} and $K_\tau = K_{sym} - 6L - \frac{Q_0}{K} L$ (see Ref.[7]).

We have chosen a set of models which have different incompressibilities at large densities and different density dependences of the symmetry energy. This is clearly seen in Fig. 1 where we have plotted the pressure of symmetric nuclear matter, Fig. 1a), and the symmetry energy for densities below 0.45 fm^{-3} , Fig. 1b). In Fig. 1a) we also include the constraints obtained from the flow analysis in heavy ion collisions [39]. It is seen that NL3 and NL3 $\omega\rho$ models give a too hard EOS at large densities, which is not compatible with the constraints from heavy ion collisions. FSU is well inside the constraints and TM1 and TM1 $\omega\rho$ are just slightly above the upper limit.

The non-linear $\omega\rho$ term will only affect the symmetry energy, therefore, models that only differ by an extra non-linear $\omega\rho$ term will have the same EOS for symmetric matter. As we will show later, this behavior will have a strong effect on the high energy collective modes. With respect to the symmetry energy NL3 and TM1 have a very hard behavior at high densities while FSU is softer. The NL3 $\omega\rho$ and TM1 $\omega\rho$ models show an intermediate behavior and approach FSU when the $\omega\rho$ coupling parameter Λ_v increases. Below $\rho = 0.1 \text{ fm}^{-3}$ the softness of the symmetry energy is reversed with NL3 the softest and FSU the hardest.

In the sequel we use the formalism developed in ref. [32] where the collective modes in hot and dense symmetric nuclear matter were determined within the Vlasov equation based on the Walecka model [42]. We will use, whenever possible, the same notation. We start from the thermodynamical potential density for npe matter

Model	ρ_0	E/A	K	E_{sym}	L	K_{sym}	K_τ
FSU	0.148	-16.302	227.895	32.537	60.395	-51.415	-275.570
TM1	0.145	-16.265	279.514	36.835	110.607	33.557	-517.390
TM1 $\omega\rho, \Lambda_v = 0.01$	0.145	-16.265	279.514	34.855	85.290	-79.145	-503.986
TM1 $\omega\rho, \Lambda_v = 0.02$	0.145	-16.265	279.514	33.235	67.654	-97.150	-434.142
TM1 $\omega\rho, \Lambda_v = 0.03$	0.145	-16.265	279.514	31.880	55.082	-72.164	-346.532
NL3	0.148	-16.240	269.937	37.344	118.320	100.525	-696.129
NL3 $\omega\rho, \Lambda_v = 0.01$	0.148	-16.240	269.937	34.929	87.638	-46.2956	-636.362
NL3 $\omega\rho, \Lambda_v = 0.02$	0.148	-16.240	269.937	33.121	68.147	-53.458	-512.296
NL3 $\omega\rho, \Lambda_v = 0.03$	0.148	-16.240	269.937	31.660	55.227	-8.069	-379.915

TABLE I. Nuclear matter properties at saturation density, ρ_0 . All quantities are in MeV, except for ρ_0 , given in fm^{-3} .

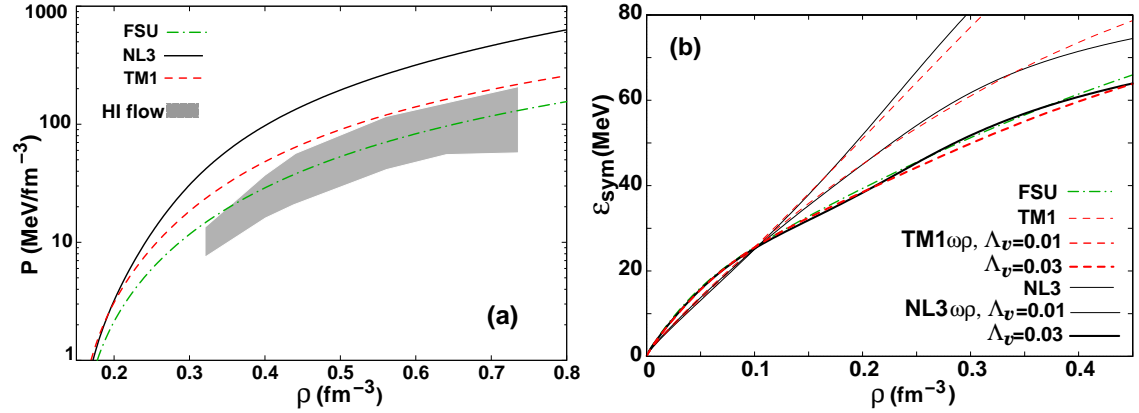


FIG. 1. (Color online) a) Pressure of symmetric nuclear matter for NL3, TM1 and FSU and b) symmetry energy for NL3 and NL3 $\omega\rho$, TM1 and TM1 $\omega\rho$, and FSU. We have considered $\Lambda_v = 0.01, 0.03$ in NL3 $\omega\rho$ and TM1 $\omega\rho$. For symmetric matter the EOS of NL3 $\omega\rho$ and TM1 $\omega\rho$ coincide respectively with NL3 and TM1. In a) we also include the constraints obtained from the flow analysis in heavy ion collisions (shaded region) [39].

where \mathcal{E} is the energy density

$$\begin{aligned}
\mathcal{E} = & 2 \int \frac{d^3p}{(2\pi)^3} \\
& [f(\mathbf{r}, \mathbf{p}, t)_+ h(\mathbf{r}, \mathbf{p}, t)_+ - f(\mathbf{r}, \mathbf{p}, t)_- h(\mathbf{r}, \mathbf{p}, t)_-] \\
& + \frac{1}{2} \left(\Pi_\phi^2 + \nabla\phi \cdot \nabla\phi + m_s^2\phi^2 + \frac{1}{3}\kappa\phi^3 + \frac{1}{12}\lambda\phi^4 \right) \\
& + \frac{1}{2} [\Pi_{V_i}^2 - 2\Pi_{V_i}\partial_i V_0 + \nabla V_i \cdot \nabla V_i \\
& - \partial_j V_i \partial_i V_j + m_v^2(\mathbf{V}^2 - V_0^2) + \frac{1}{4}\xi g_v^4(\mathbf{V}^2 - V_0^2)^2]
\end{aligned}$$

to $\phi (V_i, b_i, A_i)$, ς is the entropy density

$$\begin{aligned}
\varsigma = & 2 \sum_{i=p,n,e} \int \frac{d^3p}{(2\pi)^3} [f_{i+} \ln(f_{i+}) \\
& + (1 - f_{i+}) \ln(1 - f_{i+}) + f_{i-} \ln(f_{i-}) \\
& + (1 - f_{i-}) \ln(1 - f_{i-})]
\end{aligned} \quad (4)$$

and μ_i and ρ_i are the chemical potential and particle density of particle type i . We only consider the third component in isospin space of the ρ -meson and we denote by

$$f(\mathbf{r}, \mathbf{p}, t)_+ = \text{diag}(f_{n+}, f_{p+}, f_{e+})$$

For protons and neutrons, $i = p, n$, we have

$$\begin{aligned}\mathcal{V}_{0i} &= g_v V_0 + \frac{g_\rho}{2} \tau_i b_0 + e A_0 \frac{1 + \tau_i}{2}, \\ \mathcal{V}_i &= g_v \mathbf{V} + \frac{g_\rho}{2} \tau_i \mathbf{b} + e \mathbf{A} \frac{1 + \tau_i}{2},\end{aligned}$$

with $\tau_i = 1$ (protons) or -1 (neutrons). For electrons, $i = e$, we have

$$\mathcal{V}_{0e} = -e A_0, \quad \mathcal{V}_e = -e \mathbf{A}, \quad M_e^* = m_e.$$

The time evolution of the distribution functions is described by the Vlasov equation

$$\frac{\partial f_{i\pm}}{\partial t} + \{f_{i\pm}, h_{i\pm}\} = 0, \quad i = p, n, e, \quad (7)$$

where $\{, \}$ denote the Poisson brackets. The Vlasov equation expresses the conservation of the number of particles in phase space and, therefore, at a given temperature, the dynamics described by the Vlasov equation does not change the number of particles or antiparticles in this semiclassical approach.

From Hamilton's equations we derive the equations describing the time evolution of the fields ϕ , V^μ , A^μ , and the third component of the ρ -field, $b_3^\mu = (b_0, \mathbf{b})$, which are given in Appendix A (Eqs. (A1)-(A7)). The state which minimizes the thermodynamical potential density of npe matter is characterized by the distribution functions

$$f_{0i\pm} = \frac{1}{1 + e^{(\epsilon_{0i} \mp \nu_i)/T}}, \quad i = p, n, \quad (8)$$

with

$$\epsilon_{0i} = \sqrt{p^2 + M_i^{*2}}, \quad \nu_i = \mu_i - g_v V_0 - \frac{g_\rho}{2} \tau_i b_0 - e A_0 \frac{1 + \tau_i}{2}$$

and

$$f_{0e\pm} = \frac{1}{1 + e^{(\epsilon_{0e} \mp \mu_e)/T}}, \quad (9)$$

with

$$\epsilon_{0e} = \sqrt{p^2 + m_e^2}$$

and by the constant mesonic fields, which obey the following equations: $m_s^2 \phi_0^{(0)} + \frac{\kappa}{2} \phi_0^{(0)2} + \frac{\lambda}{6} \phi_0^{(0)3} = g_s \rho_s^{(0)}$, $m_v^2 V_0^{(0)} + \frac{1}{6} \xi g_v^4 V_0^{(0)3} + 2\Lambda_v g_v^2 g_\rho^2 V_0^{(0)} b_0^{(0)2} = g_v \mathcal{J}_0^{(0)}$, $m_\rho^2 b_0^{(0)} + 2\Lambda_v g_v^2 g_\rho^2 V_0^{(0)2} b_0^{(0)} = \frac{g_\rho}{2} \mathcal{J}_{3,0}^{(0)}$, $V_i^{(0)} = b_i^{(0)} = A^{(0)} = 0$, where $\rho_s^{(0)}$, $\mathcal{J}_0^{(0)}$, $\mathcal{J}_{3,0}^{(0)}$ are respectively

where

$$\begin{aligned}P_i &= \frac{1}{3\pi^2} \int dp \frac{p^4}{\sqrt{p^2 + M_i^{*2}}} (f_{0i+} + f_{0i-}), \\ P_l &= \frac{1}{3\pi^2} \int dp \frac{p^4}{\sqrt{p^2 + m_l^2}} (f_{0l+} + f_{0l-}), \\ P_\sigma &= -\frac{m_s^2}{2} \phi_0^{(0)2} - \frac{1}{6} \kappa \phi_0^{(0)3} - \frac{1}{24} \lambda \phi_0^{(0)4}, \\ P_\omega &= \frac{m_v^2}{2} V_0^{(0)2} + \frac{1}{24} \xi g_v^4 V_0^{(0)4}, \\ P_\rho &= \frac{m_\rho^2}{2} b_0^{(0)2}, \\ P_{\omega\rho} &= \Lambda_v g_v^2 g_\rho^2 V_0^{(0)2} b_0^{(0)2}.\end{aligned} \quad (10)$$

The chemical equilibrium conditions $\mu_p = \mu_n - \mu_e$ for neutrino free matter, or $\mu_p = \mu_n - \mu_e + \mu_{\nu_e}$ for neutrino trapped matter, as well as the electrical charge neutrality condition $\rho_e = \rho_p$ must be imposed.

Collective modes in the present approach correspond to small oscillations around the equilibrium state. These small deviations are described by the linearized equations of motion and collective modes are given as solutions of those equations. To construct them, let us define:

$$\begin{aligned}f_{i\pm} &= f_{0i\pm}^{(0)} + \delta f_{i\pm}, \\ \phi_0 &= \phi_0^{(0)} + \delta\phi, \\ V_0 &= V_0^{(0)} + \delta V_0, \quad V_i = \delta V_i, \\ b_0 &= b_0^{(0)} + \delta b_0, \quad b_i = \delta b_i, \\ A_0 &= \delta A_0, \quad A_i = \delta A_i.\end{aligned}$$

As in [27, 31, 32, 44], we express the fluctuations of the distribution functions in terms of the generating functions:

$$S_\pm(\mathbf{r}, \mathbf{p}, t) = \text{diag}(S_{p\pm}, S_{n\pm}, S_{e\pm}),$$

such that

$$\delta f_{i\pm} = \{S_\pm, f_{0,\pm}\} = \{S_\pm, p^2\} \frac{df_{0,\pm}}{dp^2}.$$

The linearized Vlasov equations for $\delta f_{i\pm}$,

$$\frac{d\delta f_{i\pm}}{dt} + \{\delta f_{i\pm}, h_{0i\pm}\} + \{f_{0i\pm}, \delta h_{i\pm}\} = 0$$

are equivalent to the following time-evolution equations:

where

$$\begin{aligned}\delta\mathcal{V}_{0i} &= g_v\delta V_0 + \tau_i\frac{g\rho}{2}\delta b_0 + e\frac{1+\tau_i}{2}\delta A_0, \\ \delta\mathcal{V}_i &= g_v\delta\mathbf{V} + \tau_i\frac{g\rho}{2}\delta\mathbf{b} + e\frac{1+\tau_i}{2}\delta\mathbf{A},\end{aligned}$$

with $h_{0i\pm} = \pm\epsilon_{0i} + \mathcal{V}_{0i}^{(0)}$ and $h_{0e\pm} = \pm\epsilon_{0e}$.

Of particular interest on account of their physical relevance are the longitudinal modes, with wave vector \mathbf{k} and frequency ω , described by the ansatz

$$\begin{pmatrix} S_{j\pm}(\mathbf{r}, \mathbf{p}, t) \\ \delta\phi \\ \delta\zeta_0 \\ \delta\zeta_i \end{pmatrix} = \begin{pmatrix} \mathcal{S}_{\omega\pm}^j(p, \cos\theta) \\ \delta\phi_\omega \\ \delta\zeta_\omega^0 \\ \delta\zeta_\omega^i \end{pmatrix} e^{i(\omega t - \mathbf{k}\cdot\mathbf{r})}, \quad (13)$$

where $j = p, n, e, \zeta = V, b, A$ represent the vector-meson fields and θ is the angle between \mathbf{p} and \mathbf{k} . The wave vector of the excitation mode, \mathbf{k} , is identified with the momentum transferred to the system through the process which gives rise to the excitation.

For the longitudinal modes, we get $\delta V_\omega^x = \delta V_\omega^y = 0$, $\delta b_\omega^x = \delta b_\omega^y = 0$ and $\delta A_\omega^x = \delta A_\omega^y = 0$. Calling $\delta V_\omega^z = \delta V_\omega$, $\delta b_\omega^z = \delta b_\omega$ and $\delta A_\omega^z = \delta A_\omega$, we will have for the fields $\delta\mathcal{V}_{i,z} = \delta\mathcal{V}_\omega^i e^{i(\omega t - \mathbf{k}\cdot\mathbf{r})}$ and $\delta\mathcal{V}_{0i} = \delta\mathcal{V}_\omega^{0i} e^{i(\omega t - \mathbf{k}\cdot\mathbf{r})}$. Replacing the ansatz (13) in Eqs. (11) and (12) we get

$$i\left(\omega \mp \frac{kp \cos\theta}{\epsilon_{0i}}\right) \mathcal{S}_{\omega\pm}^i = \mp \frac{g_s M_i^*}{\epsilon_{0i}} \delta\phi_\omega + \left[1 \mp \frac{\omega p \cos\theta}{k \epsilon_{0i}}\right] \delta\mathcal{V}_\omega^{0i}. \quad (14)$$

$$i\left(\omega \mp \frac{kp \cos\theta}{\epsilon_{0e}}\right) \mathcal{S}_{\omega\pm}^e = -e \left[1 \mp \frac{\omega p \cos\theta}{k \epsilon_{0e}}\right] \delta A_\omega^0, \quad (15)$$

In Appendix B we present the equations of motion for the field fluctuations (Eqs. (B1)-(B7)). The solutions of these equations and Eqs. (14), (15) form a complete set of eigenmodes that may be used to construct a general solution for an arbitrary longitudinal perturbation. Substituting the set of equations (B1)-(B4) into (14) and (15) we get a set of equations for the unknowns $\mathcal{S}_{\omega\pm}^i$, which lead to the following matrix equation

$$\begin{pmatrix} a_{11} & a_{12} & a_{13} & a_{14} & a_{15} \\ a_{21} & a_{22} & a_{23} & a_{24} & 0 \\ a_{31} & a_{32} & a_{33} & a_{34} & a_{35} \end{pmatrix} \begin{pmatrix} \rho_{\omega p}^S \\ \rho_{\omega n}^S \\ \rho_{\omega p} \end{pmatrix} = 0. \quad (16)$$

The eigenmodes ω of the system, with sound velocity $v_s = \omega/k$, are solutions of the Eq. (17). At subsaturation densities, there are unstable modes identified by imaginary frequencies. For these modes we define the growth rate $\Gamma = -i\omega$. The region in (ρ_p, ρ_n) space for a given wave vector \mathbf{k} and temperature T , limited by the surface $\omega = 0$, defines the dynamical spinodal surface. In the $k = 0$ MeV limit we recover the thermodynamic spinodal which is defined by the surface in the (ρ_p, ρ_n, T) space for which the curvature matrix of the free energy density is zero, i.e., has a zero eigenvalue. This relation has been discussed in [33].

III. NUMERICAL RESULTS AND DISCUSSIONS

In the present section we discuss the effect of the symmetry energy and incompressibility on some of the dynamical properties of nuclear and stellar matter. We calculate the collective modes at densities above and below saturation density and analyze their isoscalar or isovector character. We will next determine the dynamical spinodal surfaces, for different temperatures and wave vectors, characterized by a zero frequency solution of the dispersion relation (17). They will allow us to predict under which conditions a non-homogeneous phase at the crust of a proto-neutron star may exist. We will finally determine for warm β -equilibrium matter with trapped neutrinos the unstable modes with the largest growth rate, which define the mode that drives the system to a non-homogeneous phase and, therefore, gives an estimation of the size of the clusters formed in the phase transition. For these modes the magnitude of the distillation effect will be calculated. For β -equilibrium warm stellar matter with trapped neutrinos we will consider a fixed lepton fraction $Y_l = 0.4$, which corresponds to the maximum expected value [21, 45].

A. Collective modes

We have calculated at zero temperature the normal modes of asymmetric nuclear matter as a function of the nuclear matter density ρ and for different proton fractions $y_p = \rho_p/\rho$. Fig. 2 shows in the top row the ratio of the proton to neutron density fluctuations, Eq. (C3), and in the bottom row the collective mode sound velocity.

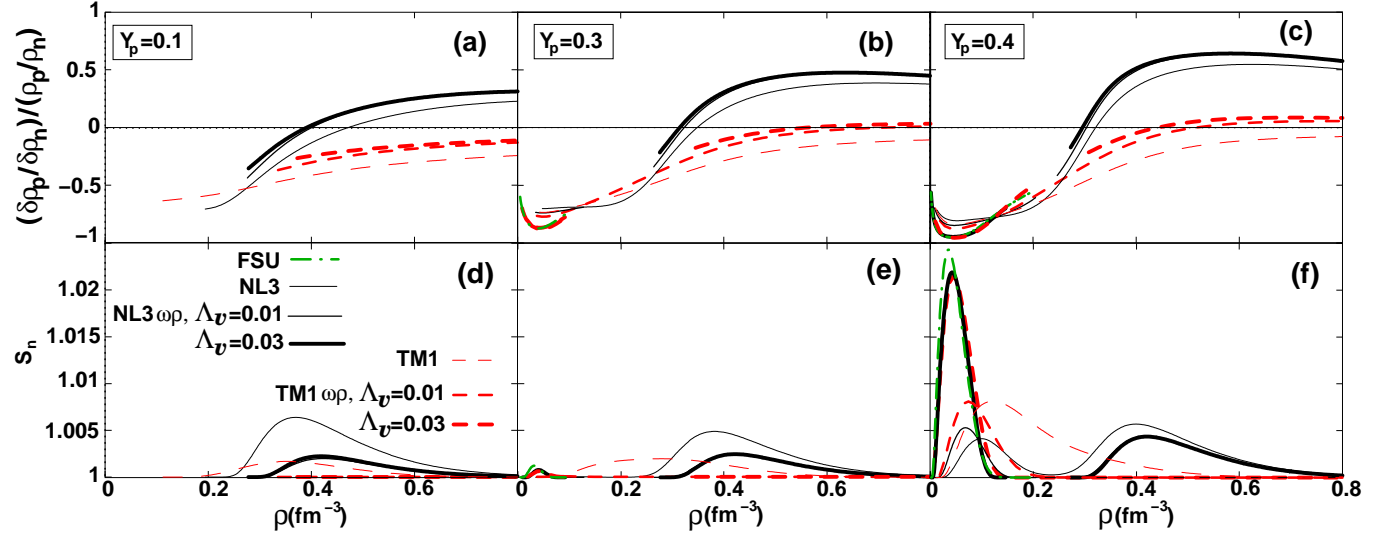


FIG. 2. (Color online) The ratio of the proton to neutron density fluctuations [Eq. (C3)] divided by the ratio of the proton to neutron densities [(a) $y_p = 0.1$, (b) $y_p = 0.3$ and (c) $y_p = 0.4$] and the sound velocity v_s normalized to the neutron Fermi velocity, $s_n = v_s/v_{Fn}$, [(d) $y_p = 0.1$, (e) $y_p = 0.3$ and (f) $y_p = 0.4$] for NL3 and NL3 $\omega\rho$, TM1 and TM1 $\omega\rho$, and FSU. $\Lambda_v = 0.01$ and 0.03 have been used in NL3 $\omega\rho$ and TM1 $\omega\rho$. The curves have been obtained for $T = 0$ MeV and $k = 200$ MeV.

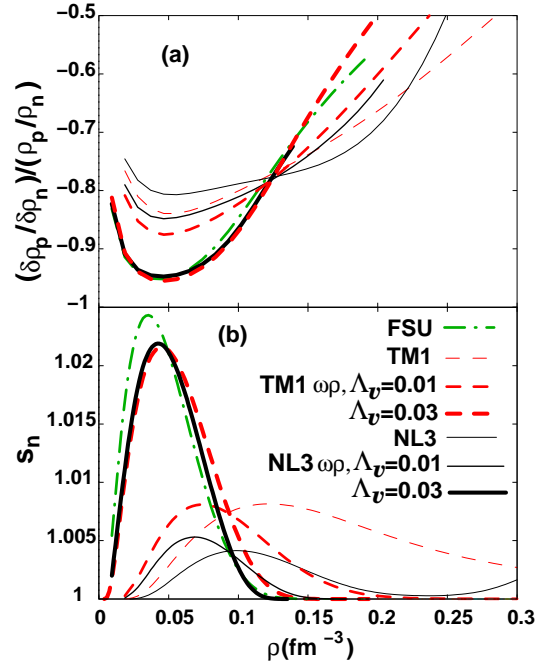


FIG. 3. (Color online) Isovector-like mode below $2\rho_0$ for $y_p = 0.4$ and $k = 200$ MeV: a) the proton to neutron density

above twice the saturation density, which we will designate by crossing density ρ_c . The crossing density decreases with an increase of the proton fraction. This is clearly seen in Fig. 4 where the crossing density is plotted for NL3 and two parametrizations of NL3 $\omega\rho$ and TM1 $\omega\rho$ ($\Lambda_v = 0.01$ and 0.03). The crossing density is sensitive to the high density dependence of the symmetry energy and, therefore, the larger the crossing density the larger the difference between NL3 and NL3 $\omega\rho$. We point out that NL3 and NL3 $\omega\rho$ only differ on the isovector channel and therefore, the differences among these models reflect the isovector behavior. TM1 has, like NL3, a very stiff symmetry energy, but, unlike NL3, has a quite soft EOS for symmetric matter at large densities due to the inclusion of quartic ω -terms. As a result the collective mode exists at large densities but with an isovector character. Including the non-linear $\omega\rho$ terms in TM1 changes this situation: for a strong enough coupling the isovector collective mode will change into an isoscalar mode, however, at much larger densities than NL3 and NL3 $\omega\rho$ models, see Fig. 4.

At very low densities the sound velocity of the modes decreases as the asymmetry increases and, as seen in Fig.2a) for $y_p = 0.1$ there are no undamped modes for

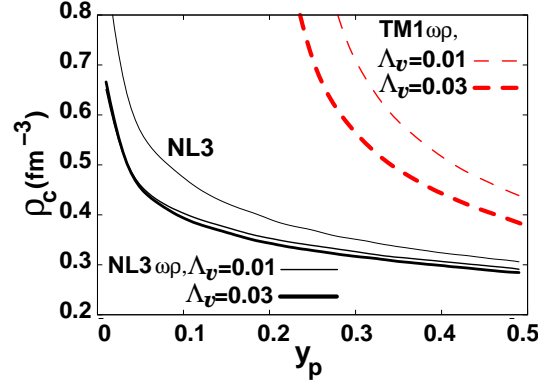
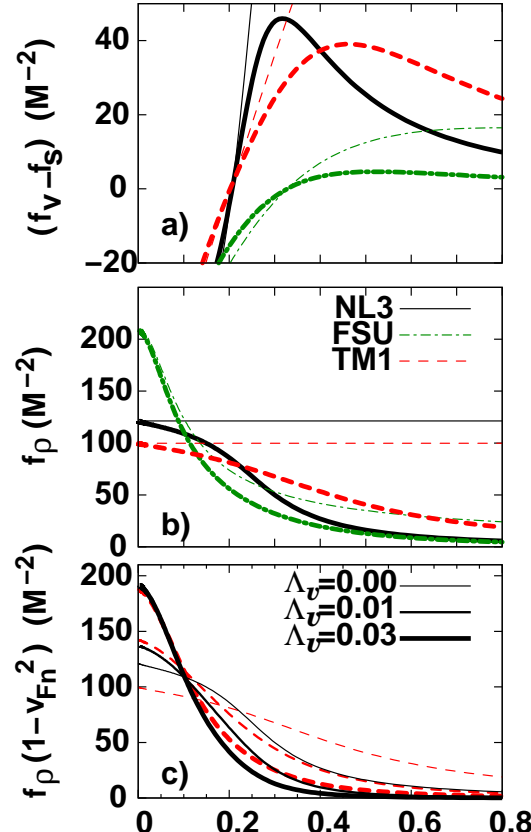


FIG. 4. (Color online) The crossing density ρ_c defining the onset of isoscalar character in the collective modes in np matter versus the proton fraction, for $k=200$ MeV and the models NL3, NL3 $\omega\rho$ and TM1 $\omega\rho$ with $\Lambda_v = 0.01, 0.03$.



high densities due to the inclusion of the δ -meson. In a similar way the isoscalar mode depends on the isoscalar response of the system and may not exist if the EOS is too soft.

The properties of the collective modes of nuclear matter described by the models introduced in the first two sections are determined by the interaction factors f_i

$$f_i = \left(\frac{g_i}{m_{i,eff}} \right)^2, \quad i = s, v, \rho, \quad (18)$$

where the effective meson masses $m_{i,eff}$ are given by

$$m_{s,eff}^2 = m_s^2 + \kappa\phi_0 + \frac{\lambda}{2}\phi_0^2 + g_s^2 \left(\frac{\partial\rho_s}{\partial M^*} \right)_0, \quad (19)$$

$$m_{v,eff}^2 = m_v^2 + \frac{\xi}{2}g_v^4 V_0^2 + 2\Lambda_v g_v^2 g_\rho^2 b_0^2, \quad (20)$$

$$m_{\rho,eff}^2 = m_\rho^2 + 2\Lambda_v g_v^2 g_\rho^2 V_0^2. \quad (21)$$

At $T = 0$ MeV, the dispersion relation (17) may be reduced to a simple analytical form for symmetric matter and in the low momentum limit [26]. If we make the approximation $v_s \approx v_F = k_F/\epsilon_F$ we get for the isoscalar mode

$$1 + 3\frac{\epsilon_F}{k_F^2}\rho \left[(f_v - f_s)(1 - v_F^2) + f_v f_s v_F^2 \frac{M^*}{\epsilon_F} \rho_s \right] \phi_s = 0 \quad (22)$$

and for the isovector mode

$$1 + \frac{3\epsilon_F}{k_F^2}\rho f_\rho(1 - v_F^2)\phi_s = 0, \quad (23)$$

where ϕ_s is the Lindhard function $\phi_s = 1 - s/2 \ln|(s+1)/(s-1)|$, $s = v_s/v_F$.

We notice that the second term of Eq. (22) is dominated by the first part proportional to $(f_v - f_s)$, while the second term of Eq. (23) strongly depends on f_ρ . Both these factors are multiplied by $1 - v_F^2 = (M^*/\epsilon_F)^2$ which approaches fast zero when the density increases. In Fig. 5 we represent these quantities: $(f_v - f_s)$ and $(f_v - f_s)(1 - v_F^2)$ in Fig. 5a) and f_ρ and $f_\rho(1 - v_F^2)$ in Fig. 5b) for NL3, TM1 and FSU, and $f_\rho(1 - v_F^2)$ for TM1 $\omega\rho$ and NL3 $\omega\rho$ in Fig. 5c). There will be an isoscalar mode only if the factor that multiplies the Lindhard function is positive. This only happens when the repulsion described by the ω -meson overcomes the σ -meson attraction, which occurs for $\rho \gtrsim 0.2$ fm $^{-3}$ for NL3 and TM1 and for $\rho \gtrsim 0.3$ fm $^{-3}$ for FSU. However, the increase of the effective mass of the ω -meson in TM1 and FSU due to the quartic ω -term in the Lagrangian density [see Eq.

and the response of the system to isovector excitations (23), which depend on f_ρ , will be significantly softened at large densities. Moreover, since the g_ρ parameter is fixed so that at $\rho = 0.1 \text{ fm}^{-3}$ the symmetry energy is the same for the models with and without the non-linear $\omega\rho$ term, the larger the coupling parameter Λ_v the larger must be g_ρ . A larger g_ρ enhances the value of f_ρ at small densities, and, therefore, also the response of the system to isovector perturbations as seen in Fig. 3: the models with the larger sound velocity and the density fluctuation ratio close to -1 are the ones with the larger f_ρ .

Comparing f_ρ with $f_\rho(1 - v_F^2)$ [Fig. 5b)], it is clear that the factor $1 - v_F^2$ makes the second term of (23) go faster to zero at large densities. TM1 has the largest values of $f_\rho(1 - v_F^2)$ at large densities which may explain its different behavior at these densities, namely the presence of an isovector like mode.

We conclude that the main role of including the non-linear $\omega\rho$ term in NL3 and TM1 is to reduce the value of f_ρ at large densities, making the isovector character of the modes weaker in this density range, and to increase the f_ρ at low densities giving rise to stronger isovector modes below $\rho \approx 0.2 \text{ fm}^{-3}$.

We stress that the above discussion refers to symmetric matter at zero temperature. In asymmetric matter isoscalar and isovector modes are coupled and we expect to find the behavior of both pure isoscalar and pure isovector modes in all modes. A stronger f_ρ ($f_v - f_s$) will give a stronger isovector (isoscalar) character to the mode.

In Fig. 6, we present the proton fractions (a) the proton-neutron density fluctuations (b) and the corresponding sound velocities of the collective modes $s_n = v_s/v_{Fn}$ (c) for β -equilibrium cold stellar matter. For the FSU parametrization we get no modes and for the parametrizations TM1 and $\text{TM1}\omega\rho$ only isovector-like modes are present. The other models change character from isovector to isoscalar at the crossing density ρ_c . The crossing density in β -equilibrium matter is almost the same for all NL3 like models although, it was seen in Fig. 2 that the crossing density depends on the isovector properties of the model. This is due to the fact that the models have different proton fractions for the same density and there are two opposite effects that define the crossing density: the larger the proton fraction the smaller the crossing density and the larger the symmetry energy at saturation the larger the crossing density. So the combination of these two effects leads to a similar

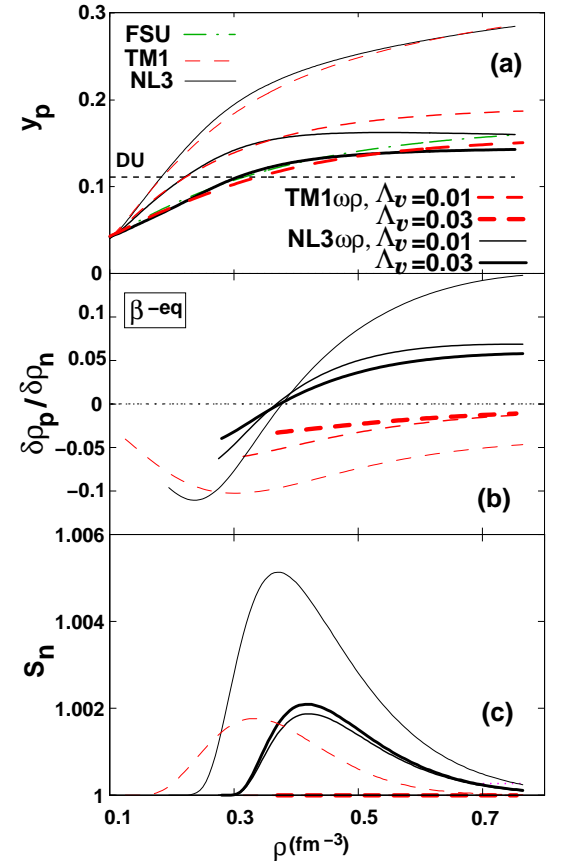


FIG. 6. (Color online) β -equilibrium stellar matter: (a) proton fraction (b) the ratio of the proton-neutron density fluctuations (Eq. (C3)) and (c) the corresponding neutron sound velocities s_n for NL3, FSU, TM1, and $\text{NL3}\omega\rho$ and $\text{TM1}\omega\rho$ with $\Lambda_v = 0.01$ and 0.03 . The results are for $T = 0 \text{ MeV}$ and $k = 200 \text{ MeV}$.

odal. The extension of the spinodal region depends on the wavelength of the perturbations: the system is stable to small wavelength perturbation, of the order of the range of the nuclear force or smaller and to large wavelengths due to the contribution of the Coulomb interaction which blows up at large wavelengths. Fig. 7 shows the approximate envelope of the spinodal regions for different temperatures and for NL3, FSU, TM1 and $\text{NL3}\omega\rho$ with $\Lambda_v = 0.01, 0.02, 0.03$. We will not consider TM1 with non-linear $\omega\rho$ because at subsaturation densities TM1 and NL3 behave in similar ways. With the increase of temperature, the spinodal region shrinks to a region

the symmetry energy.

The transition densities at the crust-core transition for β -equilibrium warm stellar matter with trapped neutrinos ($Y_l = 0.4$) are shown in Table II for several temperatures. These densities are obtained from the crossing of the EOS of β -equilibrium matter with the dynamical spinodal. The transition densities decrease with temperature due to the decrease of the spinodal region. At $T = 0$ MeV, there is no clear dependence of the transition densities on the slope L . However, if we consider the set of models that has the same isoscalar description, NL3 and NL3 $\omega\rho$, a clear tendency is seen: ρ_t decreases when L increases. This is due to the corresponding decrease of the transition proton fraction (for $T = 0$ MeV $y_p = 0.312, 0.314, 0.318, 0.322$, respectively, for NL3, NL3 $\omega\rho$ with $\Lambda_\nu = 0.01, 0.02, 1, 0.03$). A larger L corresponds to a smaller symmetry energy at subsaturation densities and allows a larger asymmetry.

In Table II we also show the transition densities for β -equilibrium neutrino-free stellar matter at $T = 0$ MeV. For neutrino-free matter, the transition densities are smaller than the ones with trapped neutrinos because neutrino free matter has a much smaller proton fraction.

The pressure has no monotonic behavior with temperature: below $T \sim 5$ MeV it increases with temperature and only above $T \sim 5 - 10$ MeV it reduces with temperature due to a large reduction of the transition density. At lower temperatures the small reduction of the transition density with respect to the $T = 0$ MeV case and a larger lepton contribution to the pressure explains the increase of the transition pressure. Similar results have been obtained in [22].

The effect of the symmetry energy slope L on the transition pressure of matter with trapped neutrinos is only clear for the set of models with the same isoscalar EOS, namely NL3 and NL3 $\omega\rho$. For these models the transition pressure increases with L at $T = 0$ MeV but does not show a systematic behavior at $T = 5$ and decreases with L at $T = 10$ MeV. At $T = 0$ MeV, the smaller isospin asymmetry for the smaller L corresponds to a smaller pressure. This tendency inverts as the temperature increases due to the larger lepton contribution to the pressure for the larger densities.

For neutrino-free matter at $T = 0$ MeV it is seen that taking the whole set of models the transition pressure does not show a clear dependence with density, in agreement with the findings of [46] with a much larger set of models. However, if we limit ourselves to the set NL3 and

pointed out that the present method of estimating the cluster size takes into account both the Coulomb interaction, which has been included in the formalism, and surface effects, which are due to the finite range of the nuclear force. Within a relativistic mean-field approach to nuclei and finite clusters surface properties are determined by the exchange of mesons with a finite mass. The estimation done with the present method agrees with the results obtained within a Thomas Fermi calculation of the pasta phase [13].

In Fig. 8 we show the cluster size estimates for matter in β -equilibrium at zero temperature. Large differences for different models can be seen for the larger densities. This is due to the fact that cold β -equilibrium matter has quite small proton fractions, for which larger differences arise between the models. It is also interesting to notice that close to the crust-core transition the clusters get larger and all models predict a size of the order of 10 fm. There is also a close correlation between the extension of the non-homogeneous phase determined by the density at which each curve ceases to exist, and the slope of the symmetry energy as noticed by many authors [7, 48]. While below $\rho = 0.02 \text{ fm}^{-3}$ all the models predict the same size of clusters, above this density there are differences between the models which are reflected in the fact that all predict similar sizes at the transition density, although this density differs from model to model.

In Fig. 9 we plot the proton over neutron density fluctuations, normalized to their corresponding ρ_p/ρ_n ratios for the largest unstable mode (first row), the corresponding growth rates (second row) and the estimated size of the clusters (third row) in β -equilibrium stellar matter with trapped neutrinos for $T = 5, 10$ and 12 MeV. These unstable isoscalar modes, since protons and neutrons fluctuations are in phase, are the ones that drive the system to a separation into a dense symmetric phase and a neutron rich gas. They are different from the isovector modes represented in Fig. 2 at subsaturation densities, for which neutron fluctuations are larger than proton fluctuations. This property has already been pointed out in [26].

When the temperature is increased, the ratio of proton-neutron density fluctuations decreases as well as the density range for clusterization. On the other hand, there is an increase of the average size of the clusters. From the top row of Fig. 9 we conclude that for warm stellar matter with trapped neutrinos, FSU and NL3 $\omega\rho$ are less effective in recovering the isospin symmetry in the liquid

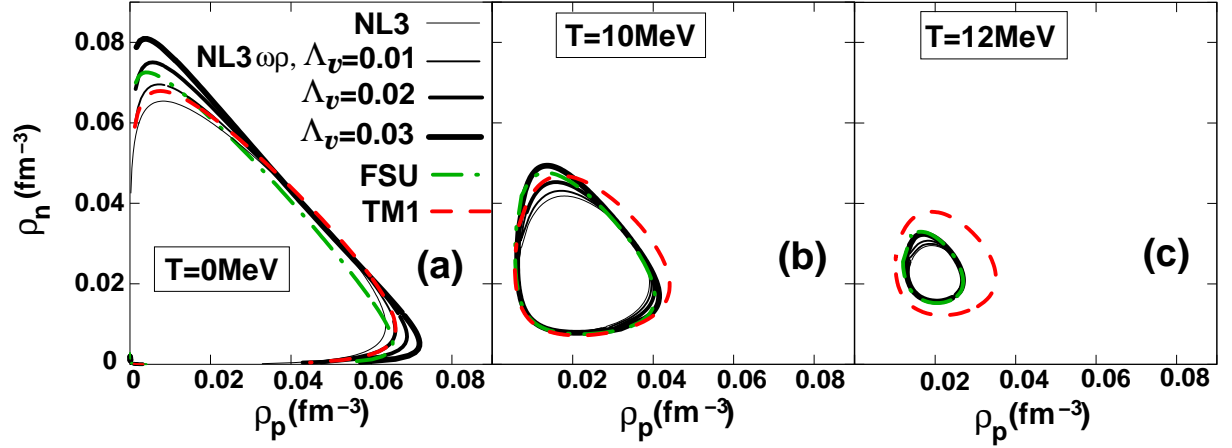
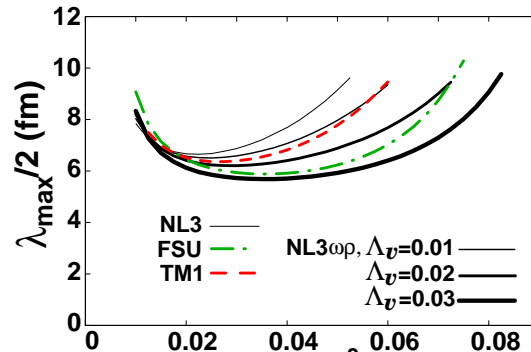


FIG. 7. (Color online) Spinodals (Eq.(17), with $\omega = 0$) for $k = 75$ MeV for NL3, FSU, TM1 and NL3 $\omega\rho$ with $\Lambda_\nu = 0.01, 0.02$ and 0.03 at a) $T = 0$, b) $T = 10$ and c) $T = 12$ MeV.

$T(\text{MeV})$		ρ_t (fm^{-3})						P_t (MeV/fm^3)					
		NL3 $\omega\rho$			NL3 $\omega\rho$			NL3 $\omega\rho$			NL3 $\omega\rho$		
		Λ_ν			Λ_ν			Λ_ν			Λ_ν		
		FSU	TM1	NL3	0.01	0.02	0.03	FSU	TM1	NL3	0.01	0.02	0.03
$Y_\nu=0$	0	0.0745	0.0602	0.0538	0.0619	0.0741	0.0855	0.388	0.324	0.236	0.357	0.500	0.535
$Y_i=0.4$	0	0.0814	0.0829	0.0816	0.0828	0.0840	0.0850	0.665	0.844	0.865	0.838	0.802	0.732
	5	0.0789	0.0803	0.0781	0.0795	0.0809	0.0821	1.021	1.064	1.087	1.074	1.086	1.090
	10	0.0652	0.0671	0.0605	0.0621	0.0642	0.0667	1.059	1.097	0.971	1.022	1.061	1.102
	12	0.0475	0.0545	-	-	-	-	0.842	0.969	-	-	-	-

TABLE II. The transition densities and the pressures for NL3, TM1, FSU and NL3 $\omega\rho$ with $\Lambda_\nu = 0.01, 0.02, 0.03$ at the crust-core transition for β -equilibrium neutrino-free stellar matter ($Y_\nu=0$) at $T = 0$ MeV and for β -equilibrium stellar matter with trapped neutrinos ($Y_i = 0.4$) for several temperatures.



[13]). There, a simple approach was used to determine the clusters: a zero surface thickness ansatz for the clusters was used with a non self-consistent surface energy. It is, therefore, important to understand this point by describing the clusterized phase within a finite temperature self-consistent Thomas-Fermi calculation. In the approach used here the increase of cluster sizes with temperature is a consequence of the fact that the smaller wavelengths do not give rise to instabilities when temperature increases. At $T = 12$ MeV only TM1 and FSU models predict the formation of clusters. Globally, the effect of the temperature on the clusterization is to increase the size of the clusters and to decrease the number of clusters per unit volume.

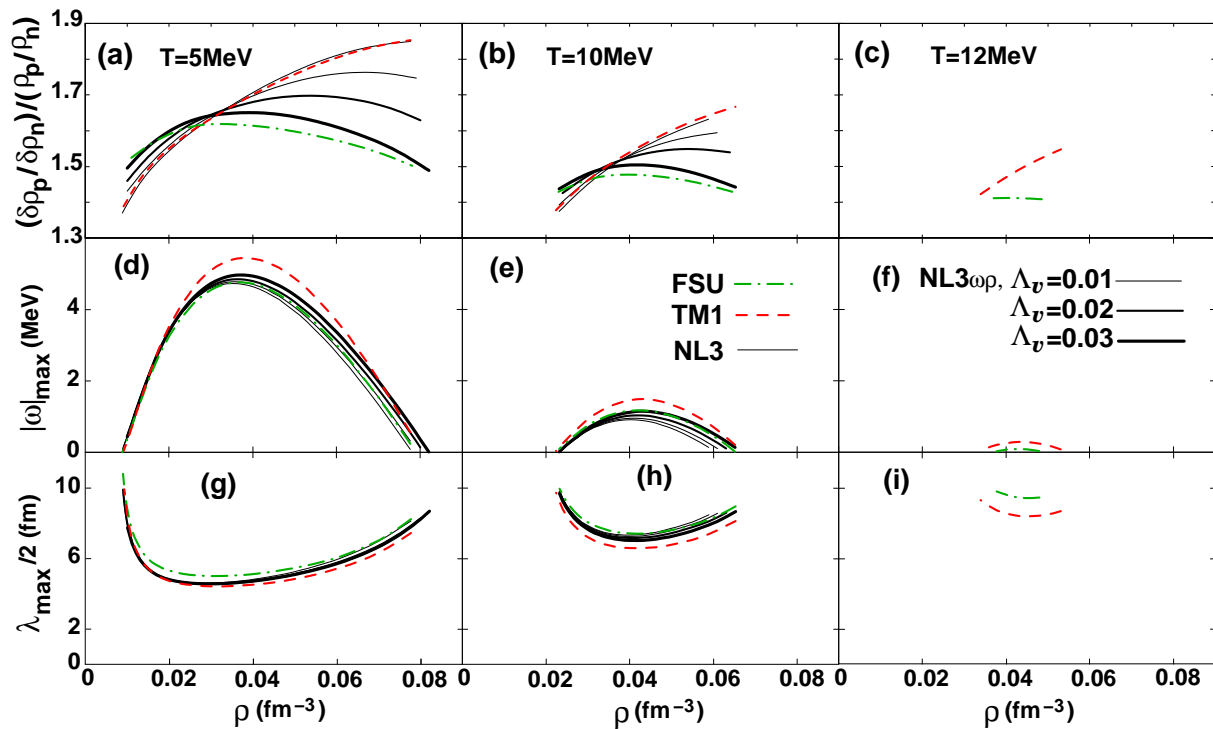


FIG. 9. (Color online) β -equilibrium neutrino-trapped matter ($Y_l = 0.4$): the normalized ratio of the proton over the neutron density fluctuations for the most unstable mode (largest $|\omega|$) at (a) $T = 5$, (b) $T = 10$ and (c) $T = 12$ MeV; the corresponding growth rates at (d) $T = 5$, (e) $T = 10$ and (f) $T = 12$ MeV and estimated sizes of the clusters at (g) $T = 5$, (h) $T = 10$ and (i) $T = 12$ MeV for NL3, FSU, TM1 and NL3 $\omega\rho$ with $\Lambda_\nu = 0.01, 0.02$ and 0.03 .

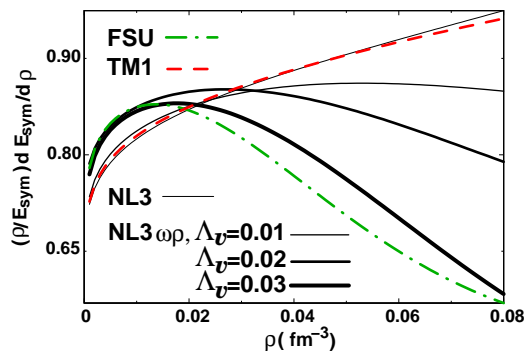


FIG. 10. (Color online) The ratio $\frac{\rho}{\mathcal{E}_{sym}} \frac{d\mathcal{E}_{sym}}{d\rho}$ at subsaturation densities for the models under study.

much.

where \mathcal{F}'' is the second derivative of the free energy density of symmetric matter with respect to the density. Since the isoscalar contribution of the different models does not differ much at subsaturation densities we may expect that the different behavior between the models is determined by the ratio $\rho (d\mathcal{E}_{sym}/d\rho)/\mathcal{E}_{sym}$. We have plotted this quantity for the range of densities of interest to understand the nonhomogenous phase. We conclude that this quantity seems also to define the behavior of the ratio of the proton to neutron density fluctuations of the most unstable mode in a dynamical approach to the instabilities of asymmetric nuclear matter.

IV. CONCLUSIONS

In the present work we have compared normal modes properties described by several relativistic nuclear mod-

neutral npe matter. We have considered a) collective modes at zero temperature, both isovector and isoscalar-like, in a wide range of densities and isospin asymmetries b) unstable modes at subsaturation densities for both cold and warm matter. We have analyzed the effect of the isovector properties, namely the density dependence of the symmetry energy, on the collective modes. All models have an isovector-like mode for densities $\rho < 0.2 \text{ fm}^{-3}$ and $y_p \gtrsim 0.25$. However, when the proton fraction decreases this mode becomes weaker and exists in a smaller range of densities. Models with a smaller symmetry energy slope have a stronger mode with a larger sound velocity. It was shown that this was due to the larger coupling factor f_ρ these models have at subsaturation densities.

For $\rho > 0.2 \text{ fm}^{-3}$, FSU has no collective mode. The parametrization TM1 has a mode which keeps always its isovector-like character, also for very high densities. For NL3, NL3 $\omega\rho$ and TM1 $\omega\rho$ the modes change from isovector-like to isoscalar-like for a density above 0.2 fm^{-3} that depends both on the model and the proton fraction. At the crossing the collective mode is a neutron wave. This feature was first identified in [26]. The differences among the models are due to the different behaviors at large densities of their effective coupling constants f_i and the nucleon effective mass M^* . A finite temperature calculation of these modes should be performed because it may affect the evolution of a proto-neutron star with trapped neutrinos.

For β -equilibrium cold neutrino free matter FSU has no collective mode, TM1 has an isovector mode for all densities above $\sim 0.11 \text{ fm}^{-3}$, NL3 and NL3 $\omega\rho$ have a collective mode respectively above 0.15 and 0.3 fm^{-3} which changes from an isovector to an isoscalar-like mode at $\rho \sim 0.4 \text{ fm}^{-3}$. It is seen that the models considered predict quite different dynamical responses.

Next we have studied the unstable modes which all models present at subsaturation densities, both for cold and warm matter. The dynamical instability density region defines a lower bound for the non-homogeneous matter in the crust of a compact star [12, 14, 15]. We have compared the predictions of the different models for cold β -equilibrium matter and warm β -equilibrium matter with trapped neutrinos. It was shown that the non-homogeneous phase could extend to $\sim 12 \text{ MeV}$ in some models but at $T = 10 \text{ MeV}$ all models predicted still a pasta phase. While the extension of cold β -equilibrium matter is model dependent and shows a close correlation

smaller distillation effect and, therefore, a proton richer background gas. This will have an effect at the level of transport properties such as electrical conductivity. It was also shown that the average cluster size increases with temperature. For cold β -equilibrium matter the average cluster size at the crust-core transition density does not depend on the model and is 10 fm large. However, because the transition density varies with the model there is quite a dispersion on the average cluster size above 0.02 fm^{-3} : the models with the larger pasta extension predict smaller clusters, $\sim 6 \text{ fm}$, for a wider range of densities. It was also shown that while the transition density decreases systematically with the increase of temperature, the transition pressure increases until $T \sim 5 \text{ MeV}$ and decreases for larger temperatures. No systematic behavior of the transition pressure with the symmetry energy slope L was obtained if the whole set of models is considered both for neutrino-free matter and neutrino trapped matter. However, taking the set of models with the same isoscalar EOS, NL3 and NL3 $\omega\rho$, we could show that for neutrino-trapped matter at $T = 0 \text{ MeV}$ the pressure decreases when L decreases due to the smaller isospin asymmetry, at $T = 5 \text{ MeV}$ there was no systematic behaviour due to a competition between the lepton contribution and the nucleon EOS and at $T = 10 \text{ MeV}$ the pressure decreases with an increase of L due to the smaller lepton contribution, for the smaller densities.

We conclude that transport coefficients of stellar matter will be sensitive to the density dependence of both the EOS of symmetric matter and the density dependence of the symmetry energy and may be used to set constraints on the EOS of cold and warm stellar matter.

Appendix A: Equations for the fields

$$\frac{\partial^2 \phi}{\partial t^2} - \nabla^2 \phi + m_s^2 \phi + \frac{\kappa}{2} \phi^2 + \frac{\lambda}{6} \phi^3 = g_s \rho_s(\mathbf{r}, t), \quad (\text{A1})$$

$$\begin{aligned} \frac{\partial^2 V_0}{\partial t^2} - \nabla^2 V_0 + m_v^2 V_0 + \frac{1}{6} \xi g_v^4 V_0 (V_\nu V^\nu) \\ + 2g_v^2 g_\rho^2 \Lambda_v V_0 (b_\nu b^\nu) = g_v j_0(\mathbf{r}, t), \end{aligned} \quad (\text{A2})$$

$$\frac{\partial^2 V_i}{\partial t^2} - \nabla^2 V_i + m_v^2 V_i + \frac{1}{6} \xi g_v^4 V_i (V_\nu V^\nu)$$

$$\frac{\partial^2 A_0}{\partial t^2} - \nabla^2 A_0 = e[j_{0p}(\mathbf{r}, t) - j_{0e}(\mathbf{r}, t)], \quad (\text{A6})$$

$$\frac{\partial^2 A_i}{\partial t^2} - \nabla^2 A_i = e[j_{ip}(\mathbf{r}, t) - j_{ie}(\mathbf{r}, t)], \quad (\text{A7})$$

where the scalar density is

$$\begin{aligned} \rho_s(\mathbf{r}, t) &= 2 \sum_{i=p,n} \int \frac{d^3 p}{(2\pi)^3} (f_{i+}(\mathbf{r}, \mathbf{p}, t) + f_{i-}(\mathbf{r}, \mathbf{p}, t)) \frac{M_i^*}{\epsilon_i} \\ &= \rho_{sp} + \rho_{sn} \end{aligned}$$

and the isovector density is

$$\begin{aligned} \rho_{3s}(\mathbf{r}, t) &= 2 \sum_{i=p,n} \int \frac{d^3 p}{(2\pi)^3} \tau_i (f_{i+}(\mathbf{r}, \mathbf{p}, t) + f_{i-}(\mathbf{r}, \mathbf{p}, t)) \frac{M_i^*}{\epsilon_i} \\ &= \rho_{sp} - \rho_{sn}. \end{aligned}$$

The components of the baryonic four-current density are

$$\begin{aligned} j_0(\mathbf{r}, t) &= 2 \sum_{i=p,n} \int \frac{d^3 p}{(2\pi)^3} (f_{i+}(\mathbf{r}, \mathbf{p}, t) - f_{i-}(\mathbf{r}, \mathbf{p}, t)) \\ &= \rho_p + \rho_n, \end{aligned}$$

$$\mathbf{j}(\mathbf{r}, t) = 2 \sum_{i=p,n} \int \frac{d^3 p}{(2\pi)^3} (f_i(\mathbf{r}, \mathbf{p}, t) + f_{i-}(\mathbf{r}, \mathbf{p}, t)) \frac{\mathbf{p} - \mathbf{V}_i}{\epsilon_i},$$

$$j_{0e}(\mathbf{r}, t) = 2 \int \frac{d^3 p}{(2\pi)^3} (f_{e+}(\mathbf{r}, \mathbf{p}, t) - f_{e-}(\mathbf{r}, \mathbf{p}, t)),$$

$$\mathbf{j}_e(\mathbf{r}, t) = 2 \int \frac{d^3 p}{(2\pi)^3} (f_{e+}(\mathbf{r}, \mathbf{p}, t) + f_{e-}(\mathbf{r}, \mathbf{p}, t)) \frac{\mathbf{p} + e\mathbf{A}}{\epsilon_e},$$

and the components of the isovector four-current density are

$$\begin{aligned} j_{3,0}(\mathbf{r}, t) &= 2 \sum_{i=p,n} \int \frac{d^3 p}{(2\pi)^3} \tau_i (f_{i+}(\mathbf{r}, \mathbf{p}, t) - f_{i-}(\mathbf{r}, \mathbf{p}, t)) \\ &= \rho_p - \rho_n, \end{aligned}$$

$$\begin{aligned} \mathbf{j}_3(\mathbf{r}, t) &= 2 \sum_{i=p,n} \int \frac{d^3 p}{(2\pi)^3} \frac{\mathbf{p} - \mathbf{V}_i}{\epsilon_i} \\ &\quad \times \tau_i (f_{i+}(\mathbf{r}, \mathbf{p}, t) + f_{i-}(\mathbf{r}, \mathbf{p}, t)), \end{aligned}$$

$$\delta\rho_i = \int \frac{d^3 p}{(2\pi)^3} p \cos\theta \left[S_{\omega+}^i \frac{df_{0i+}}{dp^2} - S_{\omega-}^i \frac{df_{0i-}}{dp^2} \right]$$

with

$$\frac{df_{0i\pm}}{dp^2} = \frac{1}{2T\epsilon_{0i}} f_{0i\pm} (f_{0i\pm} - 1)$$

the equations of motion for the field fluctuations read

$$(\omega^2 - k^2 - m_{s,eff}^2) \delta\phi_\omega = 4ig_s k \sum_{i=p,n} M_i^* \delta\rho_{si} \quad (\text{B1})$$

$$\begin{aligned} (\omega^2 - k^2 - m_{v,eff}^2) \delta V_\omega^0 &= 4g_v^2 g_\rho^2 \Lambda_v V_0^{(0)} b_0^{(0)} \delta b_\omega^0 \\ &\quad + 4ig_v k \sum_{i=p,n} \delta\rho_i, \end{aligned} \quad (\text{B2})$$

$$\begin{aligned} (\omega^2 - k^2 - m_{\rho,eff}^2) \delta b_\omega^0 &= 4g_v^2 g_\rho^2 \Lambda_v V_0^{(0)} b_0^{(0)} \delta V_\omega^0 \\ &\quad + 2ig_\rho k \sum_{i=p,n} \tau_i \delta\rho_i, \end{aligned} \quad (\text{B3})$$

$$(\omega^2 - k^2) \delta A_\omega^0 = 4iek \sum_{i=p,e} (-1)^{n_i} \delta\rho_i, \quad (\text{B4})$$

and from the continuity equation for the density currents, we get for the components of the vector fields

$$\omega \delta V_\omega^0 = k \delta V_\omega, \quad (\text{B5})$$

$$\omega \delta b_\omega^0 = k \delta b_\omega, \quad (\text{B6})$$

$$\omega \delta A_\omega^0 = k \delta A_\omega. \quad (\text{B7})$$

Appendix C: Solutions for the eigenmodes and the dispersion relation

We define the following quantities

$$\bar{\omega} = \frac{\omega}{k}, \quad x = \frac{p \cos\theta}{\epsilon_{0i}}, \quad G_\phi = \frac{g_s M^*}{k}, \quad G_\nu = \frac{g_\nu}{k}, \quad G_{\rho_i} = \frac{g_\rho \tau_i}{2k},$$

$$Z_{\omega\rho} = \frac{1}{[(\bar{\omega}^2 - \bar{\omega}_\rho^2)(\bar{\omega}^2 - \bar{\omega}_\nu^2) - D_{\omega\rho}^2]},$$

$$D_{\omega\rho} = \frac{4g_v^2 g_\rho^2 \Lambda_v V_0^{(0)} b_0^{(0)}}{k^2},$$

$$G_\phi = \frac{G_\phi^2}{\bar{\omega}^2 - 1} (k^2 + m^2)$$

$$c_e = \frac{-2}{(2\pi)^2 T} \left(\frac{e}{k}\right)^2,$$

$$I_{\omega_{\mp}}(\epsilon) = \int_{-p/\epsilon}^{p/\epsilon} dx \frac{x}{\bar{\omega} \pm x} = \pm \left[2\frac{p}{\epsilon} + \bar{\omega} \ln \left| \frac{\bar{\omega} - p/\epsilon}{\bar{\omega} + p/\epsilon} \right| \right],$$

$$I_{\omega_{\mp}}^{ni} = \int_{M_i^*}^{\infty} \epsilon^n I_{\omega_{\mp}}(\epsilon) f_{0i\mp}(f_{0i\mp} - 1) d\epsilon,$$

$$A_{\omega_i, \pm}^n = \int_{M_i^*}^{\infty} \epsilon^n d\epsilon \int_{-p/\epsilon}^{p/\epsilon} dx x S_{\omega_{\pm}}^i(x, p) f_{0i, \pm}(f_{0i, \pm} - 1),$$

$$\rho_{\omega i} = A_{\omega_{i+}}^1 - A_{\omega_{i-}}^1, \quad i = p, n, e \quad (\text{C1})$$

$$\rho_{\omega i}^S = A_{\omega_{i+}}^0 + A_{\omega_{i-}}^0, \quad i = p, n. \quad (\text{C2})$$

The coefficients a_{ij} are defined as:

$$\begin{aligned} a_{11} &= 1 + c_s (I_{\omega_+}^{0p} - I_{\omega_-}^{0p}), \quad a_{12} = c_s (I_{\omega_+}^{0p} - I_{\omega_-}^{0p}), \\ a_{13} &= -(c_{\omega}^{pp} + c_e) (I_{\omega_+}^{1p} + I_{\omega_-}^{1p}), \\ a_{14} &= -c_{\omega}^{pn} (I_{\omega_+}^{1p} + I_{\omega_-}^{1p}), \quad a_{15} = c_e (I_{\omega_+}^{1p} + I_{\omega_-}^{1p}), \\ a_{21} &= c_s (I_{\omega_+}^{0n} - I_{\omega_-}^{0n}), \quad a_{22} = 1 + c_s (I_{\omega_+}^{0n} - I_{\omega_-}^{0n}), \\ a_{23} &= -c_{\omega}^{np} (I_{\omega_+}^{1n} + I_{\omega_-}^{1n}), \\ a_{24} &= -c_{\omega}^{nn} (I_{\omega_+}^{1n} + I_{\omega_-}^{1n}), \quad a_{25} = 0, \\ a_{31} &= c_s (I_{\omega_+}^{1p} + I_{\omega_-}^{1p}), \quad a_{32} = c_s (I_{\omega_+}^{1p} + I_{\omega_-}^{1p}), \\ a_{33} &= 1 - (c_{\omega}^{pp} + c_e) (I_{\omega_+}^{2p} - I_{\omega_-}^{2p}), \\ a_{34} &= -c_{\omega}^{pn} (I_{\omega_+}^{2p} - I_{\omega_-}^{2p}), \quad a_{35} = c_e (I_{\omega_+}^{2p} - I_{\omega_-}^{2p}), \\ a_{41} &= c_s (I_{\omega_+}^{1n} + I_{\omega_-}^{1n}), \quad a_{42} = c_s (I_{\omega_+}^{1n} + I_{\omega_-}^{1n}), \\ a_{43} &= -c_{\omega}^{np} (I_{\omega_+}^{2n} - I_{\omega_-}^{2n}), \\ a_{44} &= 1 - c_{\omega}^{nn} (I_{\omega_+}^{2n} - I_{\omega_-}^{2n}), \quad a_{45} = 0, \\ a_{51} &= a_{52} = a_{54} = 0, \\ a_{53} &= c_e (I_{\omega_+}^{2e} - I_{\omega_-}^{2e}), \quad a_{55} = 1 - c_e (I_{\omega_+}^{2e} - I_{\omega_-}^{2e}). \end{aligned}$$

The ratios of the amplitudes are given by:

$$\frac{\rho_{\omega p}}{\rho_{\omega n}} = -\frac{a_{11}a_{pn} + a_{12}a_{nn} + a_{14}}{a_{11}a_{pp} + a_{12}a_{np} + a_{13} - a_{15}a_{53}/a_{55}} \quad (\text{C3})$$

with

$$a_{pp} = \frac{a_{22}a_{43} - a_{23}a_{42}}{a_{21}a_{42} - a_{22}a_{41}}, \quad a_{pn} = \frac{a_{22}a_{44} - a_{24}a_{42}}{a_{21}a_{42} - a_{22}a_{41}},$$

$$a_{nn} = \frac{a_{44}a_{21} - a_{41}a_{24}}{a_{41}a_{22} - a_{42}a_{21}}, \quad a_{np} = \frac{a_{43}a_{21} - a_{41}a_{23}}{a_{41}a_{22} - a_{42}a_{21}}$$

and

$$\frac{\rho_{\omega e}}{\rho_{\omega p}} = -\frac{a_{53}}{a_{55}}. \quad (\text{C4})$$

ACKNOWLEDGMENTS

This work was partially supported by FCT (Portugal) under grants PTDC/FIS/64707/2006, SFRH/BPD/29057/2006 and CERN/FP/109316/2009, and by COMPSTAR, an ESF Research Networking Programme. 15

- [7] I. Vidaña, C. Providência, A. Polls, and A. Rios, Phys. Rev. C **80**, 045806 (2009).
- [8] U. Garg *et al.*, Nucl. Phys. A **788**, 36 (2007).
- [9] P. Danielewicz and J. Lee, Nuclear Physics A **818**, 36 (2009).
- [10] H. Müller and B. D. Serot, Phys. Rev. C **52**, 2072 (1995); B. Li and C. Ko, Nucl. Phys. A **618**, 498 (1997); B.-A. Li, A. T. Sustich, M. Tilley, and B. Zhang, *ibid.* **699**, 493 (2002).
- [11] C. J. Pethick, D. G. Ravenhall, and C. P. Lorenz, Nucl. Phys. A **584**, 675 (1995).
- [12] K. Oyamatsu and K. Iida, Phys. Rev. C **75**, 015801 (Jan 2007).
- [13] S. S. Avancini, D. P. Menezes, M. D. Alloy, J. R. Marinelli, M. M. W. Moraes, and C. Providência, Phys. Rev. C **78**, 015802 (2008).
- [14] S. S. Avancini, L. Brito, J. R. Marinelli, D. P. Menezes, M. M. W. de Moraes, C. Providência, and A. M. Santos, Phys. Rev. C **79**, 035804 (2009).
- [15] J. Xu, L.-W. Chen, B.-A. Li, and H.-R. Ma, The Astrophysical Journal **697**, 1549 (2009).
- [16] C. Ducoin, J. Margueron, and P. Chomaz, Nuclear Physics A **809**, 30 (2008).
- [17] T. Strohmayer, H. M. van Horn, S. Ogata, H. Iyetomi, and S. Ichimaru, Astrophys. J. **375**, 679 (Jul. 1991).
- [18] J. M. Lattimer, K. A. van Riper, M. Prakash, and M. Prakash, Astrophys. J. **425**, 802 (Apr. 1994); A. Y. Potekhin, G. Chabrier, and D. G. Yakovlev, Astronomy and Astrophysics **323**, 415 (Jul. 1997), arXiv:astro-ph/9706148; E. F. Brown, The Astrophysical Journal **531**, 988 (2000).
- [19] C. J. Pethick and D. G. Ravenhall, Ann. Rev. Nucl. Part. Sci. **45**, 429 (1995).
- [20] B. Link, R. I. Epstein, and J. M. Lattimer, Phys. Rev. Lett. **83**, 3362 (1999).
- [21] M. Prakash, I. Bombaci, M. Prakash, P. J. Ellis, J. M. Lattimer, and R. Knorren, Phys. Rep. **280**, 1 (1997).
- [22] J. Xu, L.-W. Chen, C. M. Ko, and B.-A. Li, Phys. Rev. C **81**, 055805 (May 2010).
- [23] P. Haensel, Nucl. Phys. A **301**, 53 (1978).
- [24] F. Matera and V. Y. Denisov, Phys. Rev. C **49**, 2816 (May 1994).
- [25] M. Colonna, M. DiToro, and A. B. Larionov, Phys. Lett. B **428**, 1 (1998).
- [26] V. Greco, M. Colonna, M. DiToro, and F. Matera, Phys. Rev. C **67**, 015203 (2003).
- [27] S. Avancini, L. Brito, D. P. Menezes, and C. Providência, Phys. Rev. C **71**, 044323 (2005).
- [28] C. Providência, L. Brito, A. M. S. Santos, D. P. Menezes, and S. S. Avancini, Phys. Rev. C **74**, 045802 (Oct 2006).
- [29] W. Scheid, H. Müller, and W. Greiner, Phys. Rev. Lett. **32**, 741 (Apr 1974).
- [30] S. Reddy, M. Prakash, J. M. Lattimer, and J. A. Pons, Phys. Rev. C **59**, 2888 (May 1999).
- [31] M. Nielsen, C. Providência, and J. da Providência, Phys. Rev. C **44**, 209 (1991).
- [32] M. Nielsen, C. Providência, and J. da Providência, Phys. Rev. C **47**, 200 (1993).
- [33] C. Providência, L. Brito, S. S. Avancini, D. P. Menezes, and P. Chomaz, Phys. Rev. C **73**, 025805 (2006).
- [34] C. M. Ko, Q. Li, and R. Wang, Phys. Rev. Lett. **59**, 1084 (Sep 1987); C. M. Ko and Q. Li, Phys. Rev. C **37**, 2270 (May 1988).
- [35] K. Lim and C. J. Horowitz, Nuclear Physics A **501**, 729 (1989).
- [36] G. A. Lalazissis, J. König, and P. Ring, Phys. Rev. C **55**, 540 (1997).
- [37] K. Sumiyoshi, H. Kuwabara, and H. Toki, Nucl. Phys. A **581**, 725 (1995).
- [38] B. G. Todd-Rutel and J. Piekarewicz, Phys. Rev. Lett. **95**, 122501 (2005).
- [39] P. Danielewicz, R. Lacey, and W. G. Lynch, Science **298**, 1592 (2002).
- [40] M. Centelles, X. Roca-Maza, X. Viñas, and M. Warda, Phys. Rev. Lett. **102**, 122502 (2009).
- [41] J. Piekarewicz and M. Centelles, Phys. Rev. C **79**, 054311 (2009).
- [42] J. D. Walecka, Ann. Phys. **83**, 491 (1974).
- [43] S. S. Avancini, L. Brito, P. Chomaz, D. P. Menezes, and C. Providência, Phys. Rev. C **74**, 024317 (2006).
- [44] S. S. Avancini, L. Brito, D. P. Menezes, and C. Providência, Phys. Rev. C **70**, 015203 (2004).
- [45] D. P. Menezes and C. Providência, Phys. Rev. C **69**, 045801 (2004).
- [46] C. Ducoin, J. Margueron, and C. Providencia, arXiv(2010), arXiv:1004.5197 [nucl-th].
- [47] L. Brito, C. Providência, A. M. Santos, S. S. Avancini, D. P. Menezes, and P. Chomaz, Phys. Rev. C **74**, 045801 (2006).
- [48] J. Xu, L. W. Chen, B. A. Li, and H. R. Ma, Phys. Rev. C **77**, 014302 (2008).
- [49] C. Ducoin, C. Providência, A. M. Santos, L. Brito, and P. Chomaz, Phys. Rev. C **78**, 055801 (2008).